Topics in Catalysis
https://doi.org/10.1007/s11244-022-01718-y

ORIGINAL PAPER

Operando QEXAFS Study of Pt–Fe Ammonia Slip Catalysts During Realistic Driving Cycles

Vasyl Marchuk[1] · Xiaohui Huang[2,3] · Vadim Murzin[4,5] · Jan-Dierk Grunwaldt[1,6] · Dmitry E. Doronkin[1,6]

Accepted: 10 October 2022

Abstract

Bifunctional Fe–Pt ammonia slip catalysts were studied by *operando* quick-scanning extended X-ray absorption fine structure spectroscopy (QEXAFS) under conditions mimicking rapid temperature variations that occur in an automotive exhaust gas aftertreatment system during real driving. Two catalysts, Pt/Al_2O_3 and Fe-ZSM-5, were tested individually, as mixtures and in dual bed arrangements. Applying QEXAFS allowed to track changes of active metal state with high time resolution. It uncovered a strong dependence of the active metal state on reaction conditions and catalyst bed layout. For example, proximity to platinum stabilized iron species in their more active oxidized state and led to higher Fe-ZSM-5 activity. On the contrary, isolated iron species were more susceptible to overreduction by ammonia which led to deactivation and low selectivity. The use of transient conditions uncovered the influence of non-equilibrium phenomena on catalytic performance under industrially relevant conditions. Specifically, the effect of ammonia storage on the increase of activity was shown. This was also accompanied by elevated N_2O production not observed during tests with gradual heating. Additionally, unusually high NO_x selectivity was detected for Fe-ZSM-5 under these conditions. Lastly, tracking catalyst state under dynamic reaction conditions disclosed that Fe-ZSM-5 activity did not grow directly with temperature increase but rather depended on the oxidation state of Fe and surface concentration of ammonia.

Keywords Ammonia slip catalyst · Selective ammonia oxidation · Zeolite · Bifunctional catalyst · Iron · Platinum

1 Introduction

Ammonia slip catalysts (ASCs) are a component of diesel exhaust after treatment systems that oxidise residual ammonia, slipped through the NO_x selective catalytic reduction (SCR) catalyst, to nitrogen. Fe-containing zeolites are components of ASCs that are highly selective to nitrogen, but their activity is satisfactory only at temperatures above 350 °C [1]. The selectivity to nitrogen correlates with the SCR-activity of a zeolite and is especially high in the case of Fe-ZSM-5 [1]. The mechanism of ammonia oxidation on these catalysts is proposed to be so-called internal SCR (iSCR), which proceeds through initial oxidation of part of ammonia to NO_x and its further SCR by unreacted ammonia to nitrogen [2]. Activity window of Fe-containing ASCs was extended to low temperatures by combining them with noble metals (PGM), among the most active of which is platinum [3, 4]. However, this brought another problem, because such an active oxidation catalyst as Pt had significant yields of undesired N_2O and NO_x. Moreover, it converted most of NH_3 at higher temperatures to NO_x leaving insufficient

✉ Vasyl Marchuk
vasyl.marchuk@kit.edu

✉ Dmitry E. Doronkin
dmitry.doronkin@kit.edu

1 Institute for Chemical Technology and Polymer Chemistry (ITCP), Karlsruhe Institute of Technology, Engesserstr. 20, 76131 Karlsruhe, Germany

2 Institute of Nanotechnology (INT), Karlsruhe Institute of Technology, Hermann-von-Helmholtz-Platz 1, 76344 Eggenstein-Leopoldshafen, Germany

3 Department of Materials and Earth Sciences, Technische Universität Darmstadt, Alarich-Weiss-Straße 2, 64287 Darmstadt, Germany

4 Deutsches Elektronen Synchrotron (DESY), Notkestrasse 85, 22607 Hamburg, Germany

5 Bergische Universität Wuppertal, Gaußstraße 20, 42119 Wuppertal, Germany

6 Institute of Catalysis Research and Technology (IKFT), Karlsruhe Institute of Technology, Hermann-von-Helmholtz-Platz 1, 76344 Eggenstein-Leopoldshafen, Germany

Published online: 02 November 2022

amount of ammonia for the iSCR step, thus, decreasing selectivity to N_2 [5–7].

Considerable effort has been spent in the last decade to improve bifunctional ASCs containing a noble-metal and an SCR components and to unravel the factors governing their activity and selectivity. For example, different layouts of a Pt-containing component with an SCR catalyst were studied. These were mechanical mixtures of the two, their layered arrangements and even core-shell structures [8–12]. Mixed catalysts demonstrated higher selectivity to nitrogen at low temperatures, while layered catalytic beds with SCR layer upstream outperformed them by this parameter at high temperatures [8, 9, 13]. The benefit of the mechanical mixture layout was short diffusion path between two types of its active sites [9, 12, 13]. Dual layer arrangement on a monolith with a Pt-containing component downstream was improving selectivity to N_2 by enabling counter-diffusion of oxidation products from the downstream layer and ammonia from the gas feed through the outer SCR layer [11, 12, 14]. This facilitated reduction of NO_x to N_2 but decreased conversion at high flows because of a diffusion barrier in front of the active Pt-containing component [10, 12, 15]. Core-shell catalyst layout combined the benefits of the mechanical mixture and layered arrangement and provided superior N_2 selectivity both through the tight contact between the SCR and Pt-containing components and the counter-diffusion of ammonia and its oxidation products on an SCR layer [11].

Despite the outstanding advances in describing the fundamentals of combined ASCs containing a precious metal and an SCR component, there are important unresolved questions in this field. The existing studies lack characterisation of composite ASCs under working conditions. They mainly focus on explaining the varying activity and selectivity of different PGM and SCR-component arrangements with diffusion factors. However, these explanations are not exhaustive since the catalyst state, which may change significantly under reaction conditions, needs to be considered for a complete understanding of the system. Another point requiring elucidation is a possible mutual influence of Fe and Pt components on the state of each other, which could also alter the functioning of the catalytic system. Possibility of such an interaction between Fe- and Pt- components, with a probable electron transfer, was reported by Kim et al. [16]. Nonetheless, the XPS measurements of the electronic structure of Pt and Fe sites were performed ex situ and did not provide any comparison of electronic properties of Fe-Pt mixtures with individual Fe- and Pt-containing catalysts.

Another crucial factor to consider when understanding automotive exhaust gas aftertreatment catalysts is the dynamic nature of this system involving rapid temperature changes depending on the driving conditions [17–19]. As mentioned before, these changes can strongly influence exhaust catalyst structure and performance. They become especially important in the case of hysteresis, restructuring of reactive species in reaction medium or reactants storage on support [17, 20–25]. At the same time, typical catalytic studies performed in laboratory imply gradual heating in reaction mixture and may overlook the effects of these realistic rapid variations of the reactive medium. To take the dynamic conditions of driving into account, testing procedures for exhaust gas catalysts have been developed where conditions mimic real-life driving cycles [26]. The examples of such typical driving cycles for catalytic tests directly in a car are the World-wide Harmonized Light Duty Test Cycle (WLTC) or the New European Driving Cycle (NEDC) [19, 26]. It is, however, possible to implement the conditions of the automotive exhaust system occurring during driving cycles for laboratory tests or modelling in order to obtain catalyst performance resembling the one in real-life operation [19, 27–29]. Despite the importance of such an approach, it has not yet been commonly reported in general and in particular not applied to study dual-component ASCs.

In consequence, for a complete understanding of a catalyst it is necessary to describe the dynamics of the catalyst state under realistic and rapidly changing conditions. This can be achieved by applying non-invasive in situ and *operando* methods of spectroscopic analysis with sufficient time resolution. A suitable technique for such measurements has evolved from conventional X-ray absorption spectroscopy (XAS) as quick-scanning extended X-ray absorption fine structure spectroscopy (QEXAFS) and e.g. was previously successfully used to study Pt-based CO oxidation [30] or zeolite-based SCR catalysts [31].

Therefore, the aim of this work is to study different combinations of Pt/Al_2O_3 and Fe-ZSM-5 as ASCs under transient temperature conditions imitating realistic driving using *operando* QEXAFS. This will allow revealing non-equilibrium phenomena and tracking the state of Pt and Fe active species with high time resolution to correlate these with catalyst performance as function of the dynamic reaction conditions. The obtained knowledge fills the gap in the knowledge of ASCs structure in model and application-relevant conditions and facilitates their rational development in the future.

2 Experimental

2.1 Catalyst Preparation

Two Pt/Al_2O_3 catalysts were synthesised through incipient wetness impregnation (IWI). Initially, γ-alumina support (Sasol SCFa-230) was calcined at 750 °C for 4 h in air. Then the support was impregnated with a solution of Pt (II) nitrate (Chempur, anhydrous, 99.95%), dried in air for 40 h at room temperature and further for 1 h at 60 °C. The dry

impregnated sample was then calcined in static air at 400 °C (ramp rate 3 °C/min) for 4 h. After calcination the sample was reduced at 400 °C for 2 h in hydrogen flow (5% H_2 in N_2, temperature ramp rate 3 °C/min). Finally, to produce two Pt/Al_2O_3 samples with a bigger and a smaller particle sizes, one part of the reduced catalyst from the previous stage was calcined in air flow for at 500 °C, and another part—at 700 °C for 4 h in both cases (heating rate 5 °C/min). Pt loading amounted to 2 wt%. The samples are named PtA-IW-500 and PtA-IW-700, respectively.

The Fe-zeolite sample was synthesised with ion exchange using ZSM-5 as a support. NH_4-ZSM-5 (Si/Al = 11, Clariant) zeolite was dried at 150 °C for 16 h in air. 25 g of the dried zeolite were added to 2000 ml of 0.05 M $FeCl_2$ solution (prepared of anhydrous $FeCl_2$, Alfa Aesar, 99.5%). Next, ion exchange was conducted with magnetic stirring at room temperature in N_2 flow for 24 h. After its completion, the sample was filtered and rinsed with 2 l of deionised water. The filtered residue was dried in air flow at room temperature for 16 h and then—for 6 h at 120 °C. The dried sample was calcined at 500 °C for 5 h (ramp rate of 4 °C/min). Previously this preparation method resulted in about 1.3 wt% Fe loading. [23].

Four different layouts were used to combine Pt/Al_2O_3 and Fe-ZSM-5 in a catalyst bed and are shown in Fig. 1. Two of these combinations contained subsequent catalytic beds of the individual catalysts starting either with Pt/Al_2O_3 or with Fe-ZSM-5. The dual catalytic bed with Pt/Al_2O_3 upstream will be further referred to as DB Pt upstream. Correspondingly, the dual catalytic bed with Fe-ZSM-5 upstream will be named as DB Fe upstream. The other two combinations were the mixtures of Pt/Al_2O_3 and Fe-ZSM-5. One of them was the mixture of granules of separately granulated Pt/Al_2O_3 and Fe-ZSM-5, referred to simply as mixture of granules. For forming another mixture, the powders of the individual catalysts were mechanically mixed and ground together in a mortar with subsequent granulation (1:1 mass ratio). This combination of catalysts will be further named mechanical mixture.

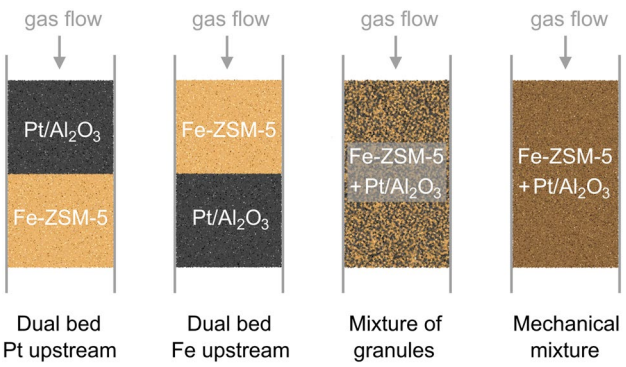

Fig. 1 Schematic illustration of catalytic beds with different Pt/Al_2O_3 and Fe-ZSM-5 layouts. From the left to the right: dual bed with Pt upstream, dual bed with Fe upstream, mixture of granules of two catalysts, mechanical mixture of two catalysts

2.2 Characterisation

The Pt/Al_2O_3 samples were characterised by transmission electron microscopy (TEM) and PtA-IW-500—by X-ray absorption spectroscopy (cf. Sect. 2.4). The TEM images were taken on a Themis 300 transmission electron microscope (ThermoFisher Scientific) equipped with a probe aberration corrector, operating at 300 kV. Particle size distribution was determined using *ImageJ* software [32].

Fe-ZSM-5 catalyst was characterised with X-ray absorption spectroscopy (cf. Sect. 2.4) and ultraviolet-visible (UV–Vis) spectroscopy using Perking Elmer Lambda 650 equipped with a Praying Mantis diffuse reflectance accessory (Harrick). The spectra were measured with 2.0 nm slit size, 1.0 nm wavelength resolution and 0.44 s scan time per point against the Spectralon reference.

2.3 Catalytic Experiments

The laboratory catalytic experiments were conducted in a plug-flow quartz reactor in a temperature-programmed mode. The catalysts were heated from 50 to 400 °C and cooled down to 50 °C in two subsequent cycles with a ramp rate of 3 °C/min. The reaction mixture composition was 500 ppm NH_3, 13% O_2 in N_2 with a 1050 cm^3/min flow. The first cycle was used to de-green a catalyst, while the results of the second catalytic cycle are discussed in this work. For the tests of the individual Pt/Al_2O_3, 25 mg of the sample were taken. For the tests of the individual Fe-ZSM-5, the loading of 50 mg of the catalysts was used. In the case of the mechanical mixture or the mixture of granules, the total loading of the previously mixed catalysts (1:1 wt. ratio) amounted to 50 mg. In the case of the dual bed arrangements, each bed contained 25 mg of either Pt/Al_2O_3 or Fe-ZSM-5. As Pt/Al_2O_3 in the laboratory catalytic tests, sample PtA-IW-500 (the one calcined at 700 °C on the final stage) was used as more active catalyst. Before the tests, the catalysts were granulated to obtain the grain size of 100–200 µm. Silicon carbide of same sieve fraction was used for catalyst dilution to obtain gas hourly space velocity of 63,000 h^{-1}. 0.5 mm layer of glass wool was used to separate the beds in the case of the dual bed arrangements. The gas concentrations in the effluent gas mixture were determined on-line with the help of a Multigas 2030 FTIR spectrometer (MKS Instruments, USA). The ammonia conversion (X_{NH_3}) was calculated according to: $X_{NH_3} = (1 - C^{out}_{NH_3}/C^{in}_{NH_3}) \times 100\%$, where $C^{out}_{NH_3}$ and $C^{in}_{NH_3}$ are ammonia concenrations at the reactor outlet and inlet, respectively. Selectivity to products was

determined as: $S_i = n_i \times C_i/(C^{in}_{NH_3} - C^{out}_{NH_3}) \times 100\%$, where C_i is product i concentration, and n_i – number of nitrogen atoms in the coresponding product molecule. The nitrogen yield was calculated from the mass balance taking into account conversion and concentrations of other products detectable by FTIR.

2.4 *Operando* QEXAFS

The catalysts with 100–200 µm sieve fraction were tested in 1.5-mm-diameter quartz capillaries (plug flow geometry, 0.02 mm wall thickness, Markröhrchen, Hilgenberg GmbH). The catalyst bed was located between two quartz wool plugs. Transmission spectra at either the Pt L_3 absorption edge or the Fe K absorption edge were recorded in the energy range of 11,375–12,330 eV and 7040–7400 eV, respectively. These ranges contained the X-ray absorption near edge structure (XANES) region of the respective absorption edges. For energy calibration, spectra of Pt or Fe foils were recorded simultaneously with experimental spectra.

Operando QEXAFS spectra were recorded at the P64 beamline of the PETRA III synchrotron radiation source (DESY, Hamburg, Germany) [33]. A Si(111) channel-cut monochromator was used. Monochromator oscillation speed was set to 5 Hz for Pt and 1 Hz for Fe (up and down scans). The sampling rate was 500 kHz for Fe and 1 MHz for Pt. Energy correction and normalisation for individual selected spectra and reference data were conducted in *Athena* software from the *IFEFFIT* package [34]. Batch processing of QEXAFS data (linear combination analysis, LCA) were conducted using the *JAQ* software (by Oliver Müller, BU Wuppertal) [33]. The average oxidation state of iron was determined from the position of the rising edge at a normalised absorbance of 0.4 (max. error is 0.1 eV, corresponding to max. error in oxidation state of 0.03).

The amounts of the *operando*-tested samples were about 4–5 mg for both Pt/Al_2O_3 and Fe-ZSM-5 and are listed in Table 1. The catalyst bed lengths for combined Fe- and Pt-containing samples were 6–7 mm, for individual Pt/Al_2O_3 and Fe-ZSM-5 catalysts 3–4 mm. For the mechanical mixture the loading was decreased, compared to other samples, not to exceed 7 mm catalyst bed length.

Table 1 Loadings for individual Pt/Al_2O_3, Fe-ZSM-5 catalysts and their combinations. m is the mass (in mg) of either Pt/Al_2O_3 or Fe-ZSM-5 loaded to a capillary in an *operando* experiment

Sample	m, mg	
	Pt/Al_2O_3	Fe-ZSM-5
Individual Pt/Al_2O_3	5.0	–
Individual Fe-ZSM-5	–	4.0
DB Pt upstream	4.0	4.0
DB Fe upstream	4.0	4.1
Mixture of granules	4.0	5.1
Mechanical mixture	6.3	

The in situ setup was similar to the ones previously described, e.g. by Grunwaldt et al. [35]. The reaction feed gas composition was 500 ppm NH_3, 10 vol% O_2 balanced with He, the total flow rate 75 cm^3/min. For the pre-treatment of the samples subsequent light-offs from 50 to 400 °C in the reaction mixture were conducted with a heating rate of 5 °C/min. After reaching 400 °C in the first light-off, the samples were cooled down to 50 °C with a rate of 5 °C/min. After reaching 400 °C in the second light-off, the cooling was performed as fast as possible (approx. 2 min). The heating in the test cycles, imitating realistic driving conditions, was conducted according to a standard type approval test for light duty diesel vehicles: NEDC (Fig. 2), reported in earlier works (e.g. Refs. [18, 30, 31]). Leister LE Mini gas blower controlled with a Eurotherm 3216e temperature controller and custom LabVIEW scripts were used to heat the sample. The temperature was measured by a K-type thermocouple contacting a sample-containing capillary. The driving cycle program was repeated 5 times for each tested sample for QEXAFS measurements both at the Pt L_3- and Fe K-edges.

The Pt/Al_2O_3 sample used for *operando* QEXAFS tests was the one calcined at 500 °C on the final stage as the catalyst (PtA-IW-500) with smaller Pt particle size. This sample offers higher spectral changes due to larger fraction of surface Pt atoms.

The composition of the gas mixture at the outlet of the reactor was analysed on-line using a Multigas 2030 FTIR spectrometer (MKS Instruments, USA) for NH_3, N_2O, NO_x and a Thermostar GSD-320 mass spectrometer (Pfeiffer Vacuum, Germany) for nitrogen. The ion current signal of nitrogen (m/z = 28) of the mass spectrometer was normalized by the signal of He (m/z = 4) to eliminate any possible

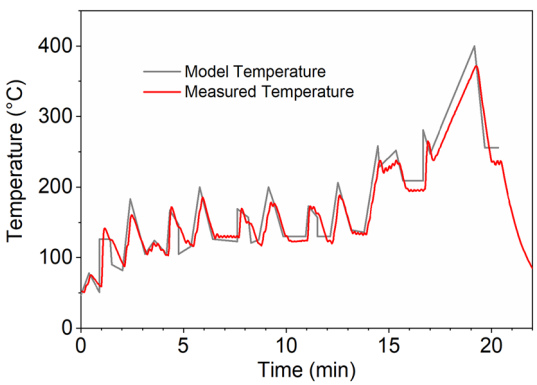

Fig. 2 Measured temperature of the experimental cycles (red) compared to temperature of model driving cycle (NEDC) based on the literature data (grey)

drift. Integral conversion of ammonia was calculated from the difference between the total NH_3 volume dosed in one cycle and the measured volume of unreacted NH_3, calculated by integration of its concentration profiles.

3 Results and Discussion

3.1 Characterisation Results

The two synthesized Pt/Al_2O_3 catalysts were characterised with TEM. According to their analysis, the Pt/Al_2O_3 sample, which was used in laboratory tests (PtA-IW-700), contained large polydisperse nanoparticles with the average diameter of 13.6 nm. The second Pt/Al_2O_3 sample, used for operando XAS measurements (PtA-IW-500), was more disperse and contained mainly 1.8 nm nanoparticles with minor fractions of clusters and single sites. Selected TEM images and the particle size distributions are shown in Fig. S1 in the supporting information (SI).

The as-prepared Fe-ZSM-5 catalyst was characterised with UV-vis spectroscopy. The UV–vis spectrum of this sample is shown in Fig. S2. The most intense band was located between 200 and 300 nm. This region is attributed to isolated Fe^{3+} ions in tetrahedral and higher coordination which, thus, were the predominant species in the catalyst [36]. Low-intensity bands on the shoulder of the main absorption band with maxima at about 350 and about 500 nm point to the presence of smaller amounts of oligomeric Fe_xO_y clusters and Fe_2O_3 particles respectively [36].

3.2 Conventional Catalytic Tests in a Laboratory Reactor

Different combinations of Pt/Al_2O_3 and Fe-ZSM-5 were tested in a laboratory reactor and compared with individual catalysts (Fig. 3A). The light-off of individual Pt/Al_2O_3 started at about 160 °C. It reached the temperature of 50% conversion ($T_{50\%}$) at 207 °C and full conversion at about 230 °C. All combinations with Fe-ZSM-5 performed similarly. However, they were more active than the individual Pt/Al_2O_3. Their $T_{50\%}$ shifted to lower temperatures and were the lowest for the mixed catalyst combinations. For the mixture of granules, $T_{50\%}$ decreased to 200 °C, and for mechanical mixture to 202 °C. Individual Fe-ZSM-5 was rather inactive compared to Pt-containing catalysts and exhibited no detectable activity under 235 °C. The sample showed a $T_{50\%}$ at 370 °C.

The differences between the individual catalysts and their combinations were more pronounced in terms of selectivity. The product distributions of the tested catalysts are shown in Fig. 3B–D. Despite all Pt–Fe combinations generally followed the selectivity trend of the individual Pt/Al_2O_3 in the lower temperature range till about 245 °C, at higher temperatures the product distribution differed. More specifically, all Pt-containing samples started with N_2 yield of about 65%. Then, after reaching full conversion, selectivity to nitrogen of individual Pt/Al_2O_3 gradually decreased to about 25%. Contrarily, N_2 yield in this range grew for 3 out of 4 Pt–Fe combinations. The selectivities to N_2 for the mechanical mixture, the mixture of granules, and DB Fe upstream had intermediate values between those of individual Pt/Al_2O_3 and Fe-ZSM-5. The latter produced almost exclusively N_2 with selectivity between 85 and 100%. The only Pt–Fe combination that did not show any improvement of selectivity to nitrogen

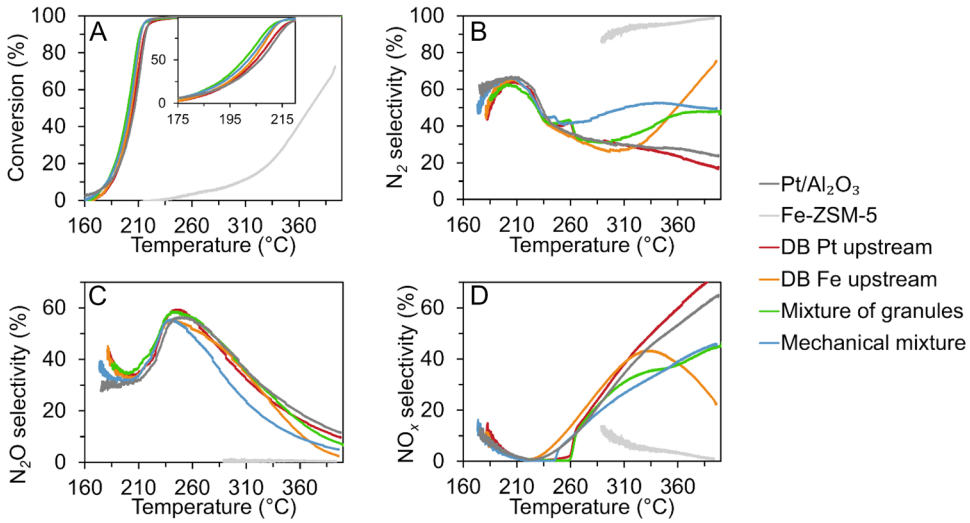

Fig. 3 Catalytic test results for the different Pt/Al_2O_3 and Fe-ZSM-5 combinations during the second heating in the reaction mixture (500 ppm NH_3 and 13% O_2 in inert, GHSV—60,000 h^{-1}). **A** Conversion; **B** selectivity to N_2; **C** selectivity to N_2O; **D** selectivity to NO_x

was DB Pt upstream. Its N_2 yield mostly followed the trend of individual Pt/Al_2O_3 and at high temperatures was even around 10% lower. Considering the three Pt-Fe combinations with improved selectivity to nitrogen, DB Fe upstream exhibited the highest N_2 yield reaching about 75%. Maximum nitrogen selectivities of both mechanical mixture and mixture of granules were lower, reaching 49% N_2 yield at 400 °C. Nonetheless, they produced an increased amount of nitrogen in a much broader range than the DB Fe upstream. For this dual bed sample, enhanced N_2 production started only above 320 °C. At the same time, the mixture of granules exhibited enhanced selectivity to nitrogen starting from 295 °C and the mechanical mixture from 245 °C. The improvement of nitrogen selectivity for all Pt–Fe combinations was mainly attained at the expense of lower selectivity to NO_x. The selectivity to N_2O was similar for individual Pt/Al_2O_3 and Pt–Fe combinations except for the mechanical mixture. This sample formed about 10% less N_2O than the Pt/Al_2O_3 above 245 °C. The abovementioned trends for both activity and selectivity were also similar during cooling down in the reaction mixture. These test results are shown in Fig. S3.

Possible explanations of varying selectivity of different Pt–Fe combinations include different mass transport patterns of the reactants and products between the two components and a potential beneficial effect of proximity of Pt and Fe sites. For example, the observation that N_2 yield did not improve in the case of DB Pt upstream may be explained with Pt/Al_2O_3 reaching full ammonia conversion before the temperatures at which Fe-ZSM-5 became active. Thus, with the lack of ammonia feed, the reduction of NO_x on Fe sites was not possible and the performance of this combination was similar to the one of the individual Pt component. On the other hand, in the case of DB Fe upstream N_2 yield was improved because NH_3 was mostly reacted on the first Fe-containing catalytic bed. However, the overall selectivity to nitrogen was lower compared to the individual Fe-ZSM-5. This can be explained with the incomplete conversion of ammonia on Fe-ZSM-5 in the whole tested temperature range, which led to further reaction of NH_3 on the second, Pt-containing, bed with some yield of the undesired products.

Using the example of the catalyst combinations in the form of mixtures, it becomes clear that the proximity of Fe species and Pt particles is beneficial for widening the temperature range of N_2 production. This proximity may decrease the diffusion length of both NO_x and unreacted NH_3 from Pt sites to Fe sites which readily catalyse SCR yielding more N_2. Thus, tight contact between Fe- and Pt-containing components in the mechanical mixture may make this effect even more pronounced than for the mixture of granules. Additionally, the mutual influence of one type of catalytic sites on another at this point becomes possible, and its role in modifying catalytic activity and selectivity needs to be assessed.

3.3 Transient Experiments Using a Spectroscopic Microreactor

3.3.1 Catalytic Results

The tests under dynamic conditions imitating realistic driving were conducted according to the protocol shown in Fig. 2. Figure 4 summarized the integral conversion of the individual catalysts and the various combinations (for details, cf. SI Figs. S4 and S5). There are significant differences in the activity of Pt–Fe combinations compared to the individual Pt/Al_2O_3 and Fe-ZSM-5 (Fig. 4). These differences were more pronounced than in the case of gradual heating during laboratory tests. For instance, DB Fe upstream and both mixtures converted approximately 1/3 more ammonia compared to the individual Pt/Al_2O_3. This is attributed to ammonia storage on the zeolite. Ammonia stored at low temperatures desorbs with rise in temperature and can be converted on Pt located downstream. This effect was not observed for the individual Pt- and Fe-containing catalysts and for DB Pt upstream. Another difference between the individual Pt/Al_2O_3 and Fe-ZSM-5 components and their combinations was their low-temperature performance. In the first 13.5 min of a cycle, at temperatures below 200 °C (until 81 min in Fig. S4), the apparent integral conversion of the individual Pt/Al_2O_3 and Fe-ZSM-5

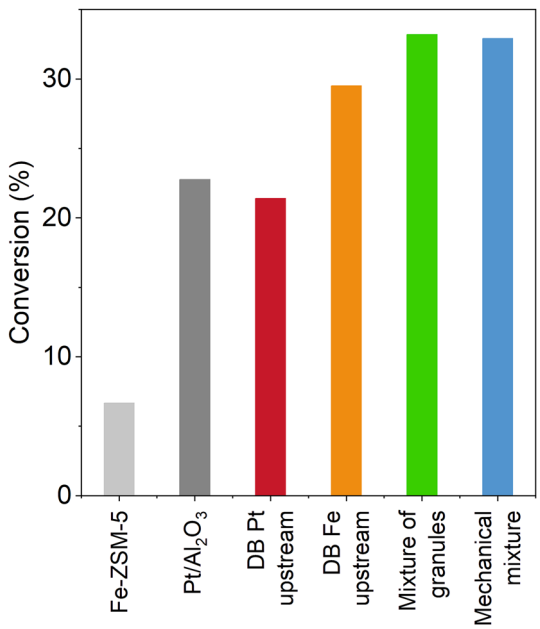

Fig. 4 Integral conversion for the different Pt/Al_2O_3 and Fe-ZSM-5 combinations during the fourth of the five subsequent transient temperature cycles imitating NEDC

was negative. This indicates that more NH_3 was thermally desorbed from these samples than converted on them. At the same time, all Pt–Fe-combinations demonstrated higher conversion in the low-temperature range of the cycle with the maximum values in the case of mixed layouts. This clearly unravels a synergy of Pt/Al_2O_3 and Fe-ZSM-5 which is enhanced through tight contact between them.

Although the trends of selectivity to nitrogen during a model driving cycle generally follow the trends observed in conventional laboratory tests, the dynamic temperature changes during driving cycles substantially alter them. These results are demonstrated in Fig. 5. As in the case of the laboratory reactor tests, mechanical mixture produced the highest integral N_2 yield (Fig. 5B, C). Most of nitrogen was observed over it during heating ramps above 220 °C. When temperature approached 275 °C, the selectivity to N_2O grew at an expense of N_2 (Fig. 6B). This nitrogen selectivity drop at high temperatures was not observed for the mixture of granules and DB Fe upstream. For this reason, although these samples did not produce as much N_2 at lower temperatures as the mechanical mixture, their overall N_2 yield was only lower by 2% and 5% for the mixture of granules and DB Fe upstream, respectively. These three Pt-Fe combinations exceeded the total production of nitrogen over individual Pt/Al_2O_3 by 15–20% and the individual Fe-ZSM-5 sample by 45–50%. As in the case of laboratory test results, DB Pt upstream did not show any improved selectivity compared to the individual Pt/Al_2O_3 and produced ~ 7% less nitrogen. Notably, none of the samples deactivated during the tests providing well-reproducible results in all model cycles (Fig. S5).

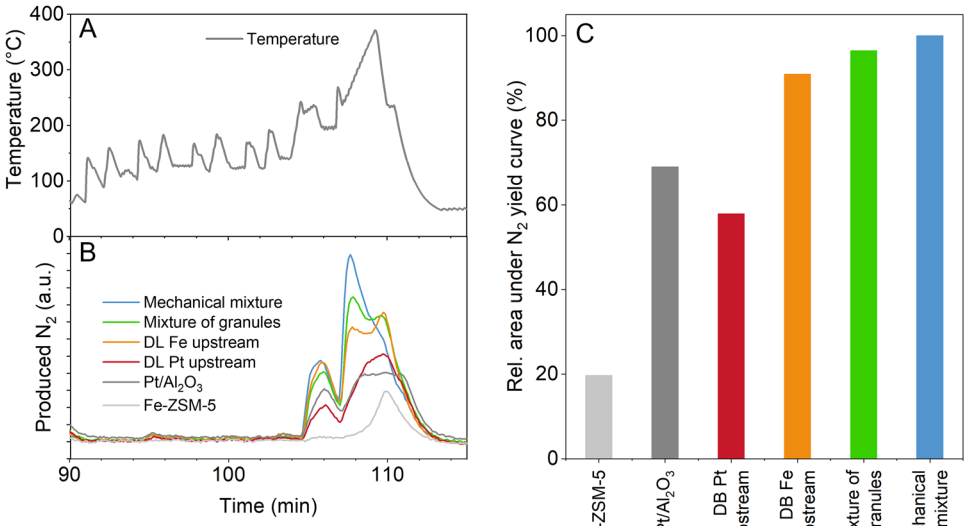

Fig. 5 Nitrogen yields for the different Pt/Al_2O_3 and Fe-ZSM-5 combinations during the fifth one of 5 subsequent cycles of temperature change imitating realistic driving. **A** Measured temperature during the cycle; **B** relative concentrations of produced nitrogen (m/z = 28) in time; **C** integral N_2 production for individual Fe-ZSM-5, Pt/Al_2O_3, and their different combinations

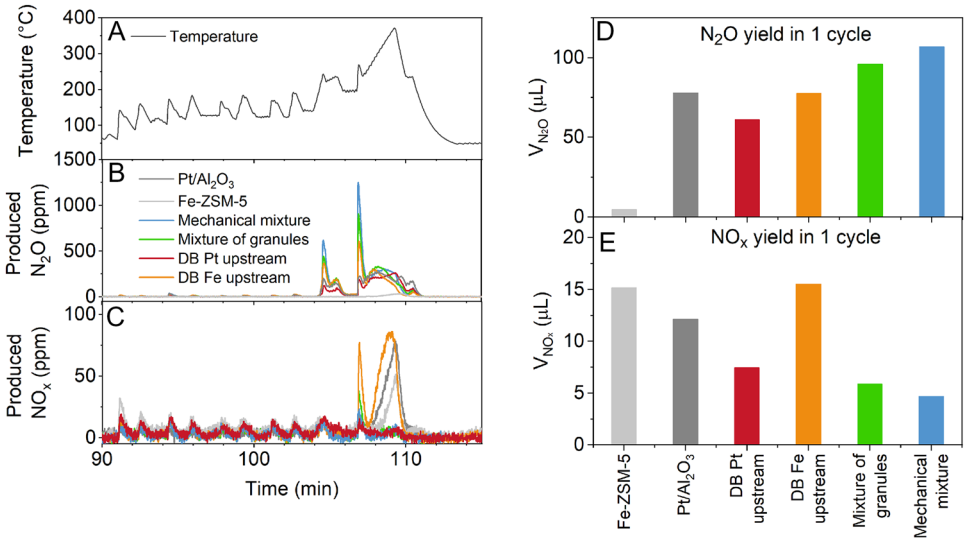

Fig. 6 By-product yields for the different Pt/Al_2O_3 and Fe-ZSM-5 combinations during the last of the 5 subsequent model NEDC cycles. **A** Measured temperature during the cycle; **B** and **C** concentration profiles of N_2O and NO_x produced during one NEDC; **D** and **E** integral N_2O and NO_x production over individual Fe-ZSM-5, Pt/Al_2O_3 and their different combinations

In contrast to N_2 selectivity, the trends of selectivity to N_2O during model driving cycles differed from those obtained in conventional laboratory tests (see Fig. 6). N_2O yields in the laboratory reactor were very similar for all Pt–Fe combinations, with the lowest one over the mechanical mixture. The latter, however, produced the highest amount of N_2O in the model NEDC cycle test. The selectivity towards N_2O was slightly lower for the mixture of granules. Their N_2O yields exceeded the one of individual Pt/Al_2O_3 by 25–30%. At the same time, DB Fe upstream was producing a comparable amount of N_2O to the individual Pt/Al_2O_3. Most of N_2O for the samples mentioned above evolved on the starts of steep heating ramps. These N_2O peaks preceded in time the corresponding peaks of N_2 production. This may serve as an indirect indication for the iSCR mechanism in which oxidation of ammonia over Pt (with N_2O as one of the significant products) precedes SCR yielding predominantly N_2. Finally, the sample DB Pt upstream did not exhibit any peak yields of nitrous oxide and produced a lower amount of N_2O than individual Pt/Al_2O_3, which can be explained with its lower conversion in general and conversion of N_2O over the downstream Fe-ZSM-5 catalytic bed.

In comparison, the observed trends of NO_x production were even more different from the laboratory results. Mechanical mixture and mixture of granules were the least selective to NO_x with less than a half of individual Pt/Al_2O_3 selectivity. DB Pt upstream produced more NO_x, but still substantially less than the individual Pt/Al_2O_3. Surprisingly, the second highest amount of NO_x was produced by the individual Fe-ZSM-5. Unlike individual Pt/Al_2O_3, it produced the main amount of NO_x not at high temperatures and high NH_3 conversions, but in the first 2/3 of the cycle, when the temperature was rapidly ramped from 60 to 180 °C. DB Fe upstream, which has the same Fe-ZSM-5 in the first bed, produced almost the same amount of NO_x. This is a remarkable observation, since individual Fe-ZSM-5 did not exhibit any activity in this temperature range in a conventional laboratory reactor. This can be hardly explained either with contamination with platinum, because for every experiment a new single-use quartz microreactor was used, and individual Pt/Al_2O_3 produced less NO_x with local overheating. All other combined Fe–Pt-containing samples demonstrated similar NO_x yields to Pt/Al_2O_3 at this part of the test cycle. A tentative explanation for such a behaviour of Fe-ZSM-5 may be some activity in ammonia oxidation of a small fraction of oxidic Fe nanoparticles that are present in the catalyst (see *Characterisation results*). According to literature, oxidic Fe nanoparticles are significantly more active in deep oxidation than isolated ionic ion sites [37]. In the conditions of rapid heating and quick desorption of ammonia, which is a poison for SCR-active single Fe sites in this reaction [23], these nanoparticles might become active and yield the observed NO_x at lower temperatures.

A closer look on the high-temperature range in the last third of the cycle (after 106 min in Fig. 6C), where NO_x yield was expected according to laboratory results, reveals a different trend. When one omits the NO_x peaks before 106 min, all catalysts enabling the diffusion of NH_3 oxidation products from Pt-containing to the Fe-containing bed, demonstrated significantly less NO_x production compared to individual Pt/Al_2O_3. The exception was the DB Fe upstream sample, in which the reaction mixture did not interact with any Fe-ZSM-5 towards the end of the catalyst bed.

3.3.2 Spectroscopic Results from *Operando* QEXAFS

The studied catalytic system can exhibit a significant gradient of concentration of reactants and products and the catalyst structure along the catalyst bed [38]. Therefore, the spectra were measured in the closest possible point to the start of a catalyst bed to probe the catalyst area with the highest concentration of the reactants in order to better track their influence on the state of the active metal under the dynamic reaction conditions.

From all Pt L_3 edge spectra recorded in parallel to the catalytic data in a model driving cycle, the strongest difference was observed between the spectra measured at the lowest and the highest temperatures. These spectra for the individual Pt/Al_2O_3 and for Pt/Al_2O_3 in mechanical mixture with Fe-ZSM-5 are shown in Fig. 7A and Fig. 7B,

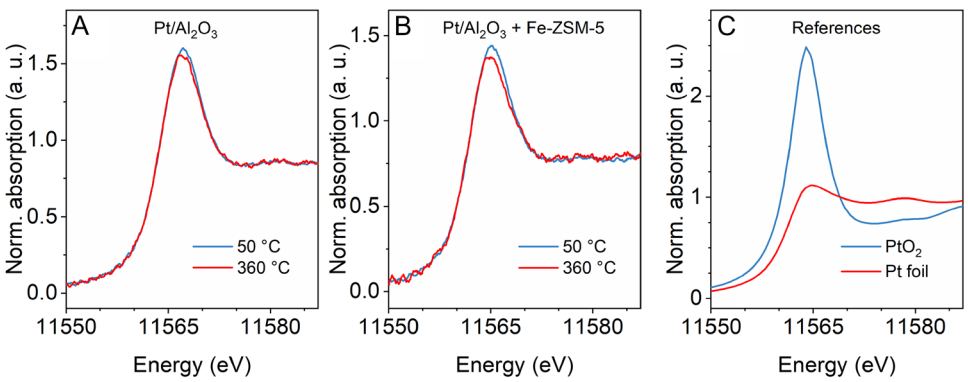

Fig. 7 *Operando* Pt L_3 edge XANES spectra with the most distinct white line shapes taken at 50 and 360 °C in the reaction feed (500 ppm NH_3 and 10% O_2 in inert): **A** for individual Pt/Al_2O_3 catalyst; **B** for Pt/Al_2O_3 in mechanical mixture with Fe-ZSM-5; **C** reference Pt spectra (note the different y-scale)

respectively. For all samples, they corresponded to Pt in intermediate oxidation states between metallic Pt and PtO_2, the reference spectra of which are presented in Fig. 7C. In both cases (individual Pt/Al_2O_3 and its mechanical mixture with Fe-ZSM-5), platinum reduction was observed as a result of heating in the reaction mixture. This is evidenced by the decrease of maximum intensity near the absorption edge (this energy range is also known as a "white line") [39]. For Pt/Al_2O_3 in mechanical mixture with Fe-ZSM-5, the white line intensity decreased more and, hence, reduction was slightly stronger. All other measured Pt L_3 spectra at temperatures in between the highest and the lowest one were located in between the two most distinct spectral shapes described above. The trends of these changes have been analysed further.

Differences in Fe K edge spectra of individual Fe-ZSM-5 and its mechanical mixture with Pt/Al_2O_3 were more pronounced. The most different shapes of the Fe K spectra were found for the individual Fe-ZSM-5 and, as in the case of Pt, for the highest and lowest temperatures (cf. Fig. 8A). The absorption edges of the iron species at both low and high temperatures were located between α-Fe_2O_3 and FeO (Fig. 8). This points to intermediate oxidation states between +2 and +3. The spectra of α-Fe_2O_3 and FeO were used as standards to estimate the average oxidation state of Fe under the respective conditions. It amounted to +2.06 at 50 °C and to +2.45 at 360 °C for the individual Fe-ZSM-5. This indicates reduction of Fe during heating in the reaction mixture. In the same way, oxidation states for the most different spectra at 50 and 360 °C were calculated for the other samples. The corresponding spectra are shown in Fig. S6, and the corresponding oxidation states—in Table S1. In contrast to the behaviour of the individual Fe-ZSM-5, the changes in the white line shape and edge position for the spectra of Fe in combination with Pt were less pronounced. This indicates a more stable oxidation state. The most evident example of Fe oxidation state stability in presence of Pt was observed for the mechanical mixture. Its spectra were almost identical at higher and lower temperatures (Fig. 8B). The oxidation states for this sample were significantly higher than for Fe-ZSM-5 and amounted to +2.50 at 50 °C and +2.59 at 360 °C. Their difference amounted to only 0.09, compared to 0.38 for the individual Fe-ZSM-5. The other samples showed trends between Fe-ZSM-5 and the mechanical mixture. Both the variance and the absolute values of their oxidation state correlated with the proximity between Fe and Pt species (see table S1). This is a clear indication that the tight contact with Pt prevented Fe from reduction by the reaction medium and stabilised it in a more oxidised state.

In order to track the change of Pt and Fe states under dynamic conditions of a typical NEDC driving cycle, the most distinct spectra for each dataset were chosen as internal references to conduct LCA. In this way, the relative fraction of the low-temperature components (more oxidized states) was determined during the NEDC with 0.2-1 s time resolution for Pt and Fe components correspondingly. The exemplary internal reference sets are shown in Figs. 7A, B and 8A, B, all used Fe K internal reference spectra are also shown in Fig. S6. The results of LCA analysis for Pt were noisy and did not exhibit clear trends (Fig. S7). Unlike Pt, LCA-derived change of Fe oxidation state demonstrated a clear correlation with the reaction conditions and the catalyst performance (Fig. S8). Therefore, an additional analysis was conducted to attribute these changes to absolute oxidation states of Fe over the whole NEDC. For this purpose, we used the previously determined oxidation state of the internal references (Table S1) and the LCA-derived contributions of these references (Fig. S6) into the measured spectra for each data point. Figure 9 juxtaposes these analysis results with the temperature program and product concentrations in one driving cycle. The same results for five cycles are shown in Fig. S9.

The change of Fe oxidation state in the dynamic reaction conditions of driving cycles (Fig. 9) appears to correlate with the catalytic activity. For example, the least active catalyst, the individual Fe-ZSM-5, exhibited pronounced reduction in the reaction mixture (by 0.38, changing between

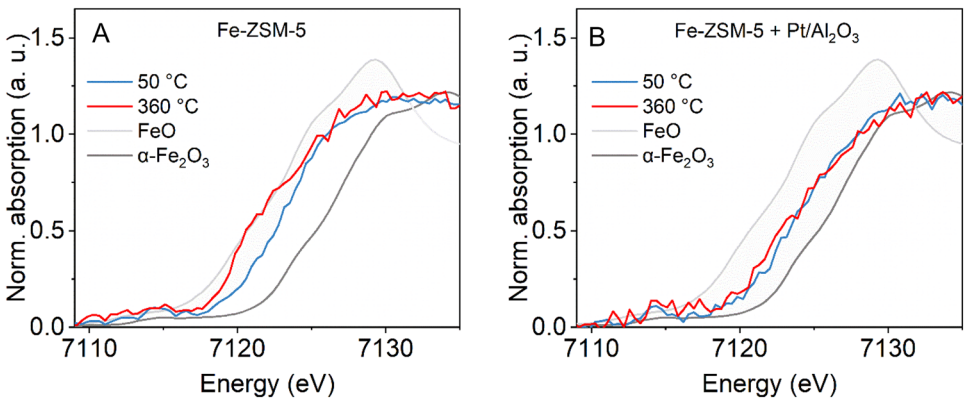

Fig. 8 *Operando* Fe K edge XANES spectra with the most distinct near edge/white line shapes taken at 50 and 360 °C in the reaction feed (500 ppm NH_3 and 10% O_2 in inert): **A** for individual Fe-ZSM-5 catalyst; **B** for Fe-ZSM-5 in mechanical mixture with Pt/Al_2O_3.

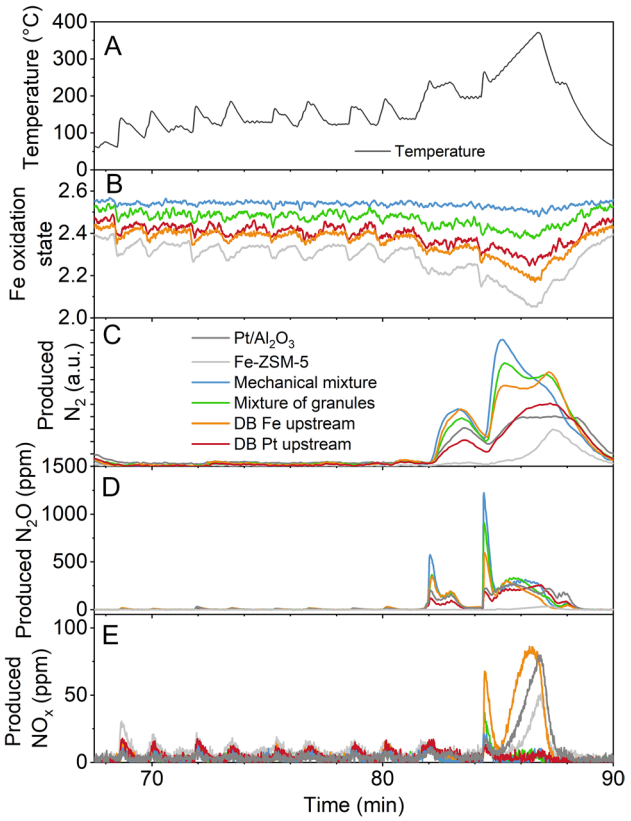

Fig. 9 Correlation of product concentrations with temperature and state of Fe during the fourth one of 5 subsequent cycles of temperature change imitating realistic driving. **A** Measured temperature during the cycle; **B** change of Fe oxidation state; **C** concentrations of N_2; **D** concentrations of N_2O, **E** concentrations of NO_x

+2.06 and +2.45; see Table S1) with temperature ramping up and re-oxidation during cooling down. Iron reduction with ammonia was previously observed in SCR reaction and attributed to a less active ammonia-poisoned catalyst state [23]. Fe-ZSM-5, thus, produced most of N_2 not at high temperature but rather during the cooling step (e.g. around 20 min in Fig. 9), when its average oxidation state increased again. Other samples with a catalytic bed of Fe-ZSM-5, DB Fe upstream and DB Pt upstream, also produced N_2 in this time span. Nevertheless, these samples produced most of N_2 earlier, during the upward heating slopes, which presumed participation of the Pt-containing beds and will be discussed further. The initial oxidation states of the dual bed catalysts were similar (+2.54 and +2.50 for the DB Pt upstream and for the DB Fe upstream, respectively), but DB Pt upstream was reduced to a lower extent to +2.28 (by 0.26), compared to 2.19 (by 0.31) for DB Fe upstream. On the other hand, the catalysts with Fe-ZSM-5 contacting with Pt/Al_2O_3—mixture of granules and mechanical mixture—were the most oxidised ones and kept a much more stable oxidation state, which proves the crucial role of tight contact of Fe and Pt sites for maintaining Fe in oxidised state. This stable oxidation state of Fe seems to be at the origin of the enhanced yield of N_2 at lower temperatures and ascending slopes of temperature ramps compared not only to the individual Fe-ZSM-5, but also to its dual bed compositions with Pt/Al_2O_3.

4 Discussion

Transient cycle testing revealed effects of ammonia storage on the zeolite-containing component. Its role may be seen, in particular, by comparing the activity and selectivity profiles of the dual component systems with those of the individual catalysts. One such example are the previously mentioned spikes in N_2O production for all dual-component systems except the DB Pt upstream (Fig. 9D). Since Fe-ZSM-5 produced almost no nitrous oxide, the peaking evolution of this by-product on steep heating ramps on 82 and 84.5 min in Fig. 9 originated from Pt, apparently from the zeolite-stored ammonia. Notably, the DB Pt upstream, where zeolite-stored ammonia evaded diffusion through the Pt/Al_2O_3 bed, demonstrated lower N_2O yield with a profile similar to the individual Pt/Al_2O_3. One more phenomenon explaining the varying activity and selectivity of the dual-component systems tested may be the synergy of the Fe- and Pt-containing components. Similarly to the DB Fe upstream, the mixtures of Fe-ZSM-5 and Pt/Al_2O_3 exhibited increased conversion on Pt in the conditions where the Fe-ZSM-5 was inactive (Fig. 9C–E, S4). This differed from the testing with gradual heating where the temperature range of the increased N_2 selectivity coincided with the range of the Fe-ZSM-5 activity (Fig. 3). Apparently, ammonia storage contributed to the conversion increase of the composites in the driving cycles. However, it does not fully explain the results for the mixtures because their NH_3 conversions exceeded the one of the DB Fe upstream and the sum of the conversions of the individual components. This clearly points to a synergy of the Pt/Al_2O_3 and Fe-ZSM-5 combination in tight contact.

Differences in catalytic performance observed during tests in driving cycles were accompanied by different trends in the oxidation state of the iron sites. More specifically, the systems with tight contact between the two active components (the mechanical mixture and mixture of granules) had the highest and the most stable iron oxidation state (Fig. 9B, Table S1). They also produced most N_2 and had the highest conversion among all tested samples, which exceeded also the sum of conversions over the individual Pt/Al_2O_3 and Fe-ZSM-5 (Figs. 5, 9C). On the contrary, the iron oxidation state in the samples with separate Fe-ZSM-5 beds changed significantly with temperature and correlated with activity and selectivity under realistic dynamic conditions. For example, in contrast to the laboratory test results, the activity of Fe-ZSM-5 did not directly grow with the temperature

increase. The *operando* spectra showed that Fe was reduced during the whole heating to 360 °C (around 86.5 min in Fig. 9) in the reaction feed and became active only when it started to re-oxidise during cooling (after 86.5 min). Apparently, the re-oxidation became possible after desorption of the excess of ammonia stored on zeolite prior to the intense heating. Another effect that can be better understood with the help of *operando* XAS is the high NO_x yield on Fe-ZSM-5 not observed during the conventional laboratory tests. It seems that the ammonia inhibition of the SCR-active Fe species during heating pulses may be responsible for such an unusual selectivity. More specifically, a rapid decrease of Fe oxidation state was clearly seen during all temperature pulses of a driving cycle (Fig. 9A, B). Additionally, the maximal NO_x yield coincided with the most reduced oxidation state of Fe at the highest temperature (360 °C around 86.5 min, Fig. 9A, B, E). These trends were also similar for DB Fe upstream, where the catalytic bed of Fe-ZSM-5 was also exposed to all ammonia dosed with the gas feed as was the individual Fe-ZSM-5. The resulting ammonia excess poisoned SCR-active Fe species and, at the same time, provided enough ammonia to unselectively react over Fe_xO_y oligomers and nanoparticles [36, 37]. Remarkably, with the stable oxidation state of Fe in tight contact with Pt in the mechanical mixture, almost no NO_x production pulses were observed. This may be another indirect confirmation of a tendency of the reduced Fe-ZSM-5 to favour nitrogen oxide production.

We should note that for precise evaluation of Fe oxidation state, the analysis of the pre-edge XANES region needs to be used, as done, for example, in Refs. [40, 41]. However, such an analysis requires high quality data which presumes high acquisition time of the spectra. For this study, high time resolution was the priority, therefore, an approach of comparing the position of the absorption edge was used. It helped to set the observed spectral changes to a relevant scale. This allowed to better distinguish the trends in the changes of the state of Fe and estimate their extent. Despite the potential bias in the determined oxidation states, the used approach allows setting a common scale for all measurements and discussing trends in the oxidation state of Fe.

Hence, with the help of *operando* XAS, a correlation of the iron oxidation state with catalytic performance was found. The rather reduced Fe species in the case of the isolated Fe-ZSM-5 were SCR-inactive allowing undesired NO_x. On the other hand, oxidised Fe sites in tight contact with Pt corresponded to higher activity and selectivity to N_2. These findings, together with the peculiar features of activity and selectivity observed in the driving cycles and absent in the tests with gradual heating, allow to specify the main factors influencing the performance of the ASCs combining Fe-zeolite and Pt/Al_2O_3: (1) ammonia storage both at low and high temperatures; (2) increased activity of Fe sites in contact with Pt; (3) efficient mass transport of NH_3 and its oxidation products either from the Pt- to Fe-containing component or in the opposite direction. The first factor, ammonia storage on Fe-ZSM-5, may reasonably well explain the enhanced conversion and N_2 yield of the dual-component systems. It plays a predominant role in the case of the DB Fe upstream sample and has already been discussed above. In order to understand the even higher activity and selectivity increase of the mixed catalyst beds, the tight contact between Fe and Pt needs to be considered.

In this study, we showed that tight contact between Pt particles and Fe sites increased low-temperature selectivity to N_2 because of the decreased ammonia poisoning effect on iron. This is an aspect that, to our knowledge, has not been reported previously. The earlier works on the topic explain the benefit of the tight contact between Pt and SCR-active sites mainly by the decrease of diffusion path length between Pt and Fe sites and, as a result, a higher chance for oxidation products and ammonia to react on an SCR-active site [9, 11, 12]. However, this study suggests that the stable oxidation state of Fe in contact with Pt may be an additional factor to explain the low-temperature activity and selectivity of the mixed catalyst arrangements. More specifically, re-oxidation of Fe was shown to be the slowest step in the SCR of NO_x by NH_3 [38]. Therefore, due to the stabilisation of Fe sites in the more oxidised state in proximity to Pt, the mechanical mixture demonstrated the highest N_2 yield, outweighing also other samples, even though some of them were more selective at high temperatures. The origins of the stable oxidised state of Fe mixed with Pt can hardly be caused by the direct contact between Pt and Fe entities. Particularly, Pt particles exceed the size of zeolite pores which host most of the Fe ions (although ion migration between the supports cannot be excluded in these systems). Hence, Pt is more likely to affect Fe sites through the products of ammonia oxidation. On the one hand, it decreases the concentration of NH_3 by converting it. On the other hand, Pt produces deep oxidation products, such as NO_2 and NO [42]. These two gases, together with ammonia, can participate in the so-called fast SCR which proceeds on Fe at low temperatures and yields N_2 [43].

On the contrary, high-temperature selectivity to N_2 required Fe-ZSM-5 separated from Pt, provided there was sufficient ammonia feed on the Fe-containing component, in accordance with earlier reports [5, 9]. Hence, the samples DB Fe upstream and the mixture of granules, which had Fe-ZSM-5 separated from Pt and enabled sufficient NH_3 feed on it, were most selective towards nitrogen among all the samples at high temperatures. The reason for such behaviour was that in these catalysts, ammonia flow reached Fe-ZSM-5 while it was exhibiting satisfactory activity and high selectivity in these high-temperature conditions (for instance, 87.5 min in Fig. 9). At the same time, for the other catalysts

most of ammonia was converted with the much more active but less selective Pt, thus, leaving no reducing agent for SCR on Fe-ZSM-5.

Finally, also NO_x production is strongly affected (Figs. 6 and 9C, E). Firstly, the samples in which oxidation products from the Pt-containing component could diffuse to the Fe-ZSM-5 catalyst, produced almost no NO_x at high temperatures, where its highest yields were expected on individual Pt (after 84 min in Fig. 9). Secondly, increased NO_x yield for the DB Fe upstream, compared to the individual Pt/Al_2O_3, may be explained with the additional total conversion because of ammonia stored on zeolite and desorbed at higher temperature. Moreover, even though the conversion on the upstream bed of Fe-ZSM-5 yielded mainly N_2, the residual ammonia, which was not completely converted on this barely active catalyst, continued its oxidation on Pt with substantial selectivity to NO_x due to the temperature increase.

It is important to note that the systems tested in this study differ from those used in industry. The primary difference is the use of powder catalysts in plug flow reactors instead of coated monoliths. In these systems, the type of mass transfer is significantly different. Particularly, in plug flow reactors convection of reactants prevails while in coated monoliths convection coupled diffusion between catalyst layers plays the major role. Additionally, monoliths are operating at significantly higher gas flows. However, employing a simplified model catalytic system was necessary for acquiring *operando* spectroscopic data, because monoliths do not allow for uniform sample thickness and sufficient transmission of X-rays at Fe K and Pt L_3 edges. Another constraint of the used approach is the use of relatively large Pt catalyst bed compared to the amount of Pt used in industrial catalysts, also dictated by the in situ cell and experiment geometry. In the case of the DB Pt upstream, high Pt content led to overconsumption of ammonia on the Pt-containing catalytic bed and did not allow the Fe-containing bed to participate in the reaction. However, the used approach allowed to gain the insight into Pt–Fe interaction in their tight contact and to compare their state in individual catalytic beds. This information can be useful for developing kinetic models based on the tests of industrial systems and can help in validating these models.

The findings obtained with the spectroscopic microreactor not only explain catalytic activity and selectivity in rapidly changing temperature conditions but also have a broader potential for applications. For example, the use of a real catalyst bed in a plug-flow geometry is an improvement, compared to the work of Benzi et al. [30], which enables obtaining kinetic information and validating micro- and macro-kinetic models. Additionally, the application of temperature profile present during real-life operation simplifies the choice of conditions for such validation, helps to prevent excessive assumptions or insufficient consideration of transient effects. Moreover, the approach used in this work can be useful not only in exhaust gas aftertreatment, but also for studying other catalytic systems with dynamic reaction conditions, for example, fuel cells or synthetic fuels production with intermittent wind or solar energy supply [44].

5 Conclusion

Pt/Al_2O_3 and Fe-ZSM-5 catalysts, their mixtures, and dual bed arrangements were tested in temperature conditions mimicking realistic automotive driving cycles and characterised by *operando* QEXAFS. The application of the temperature transient conditions allowed to unravel important aspects of catalytic activity and selectivity not present during conventional laboratory tests with gradual heating. This includes high NO_x production on Fe-ZSM-5 and elevated yields of N_2O on dual-component systems, synergy of Fe and Pt in tight contact, the influence of ammonia storage on activity and selectivity. This demonstrates the need to study catalysts also under transient reaction condition with rapid changes in gas atmosphere, temperature etc.

Operando QEXAFS allowed to follow catalyst state under these rapidly changing conditions, which resemble automotive driving cycles and to correlate it with catalytic performance. The results uncovered that tight contact with Pt promoted iron sites in the zeolite. The origin of the promotion was probably the stabilization of the iron sites in the more active oxidized state, which benefited their low-temperature activity and, hence, overall selectivity to N_2. On the contrary, rapidly changing oxidation state and fast reduction of isolated Fe-ZSM-5 catalytic bed were associated with low activity and production of NO_x during rapid heating pulses.

Supplementary Information The online version contains supplementary material available at https://doi.org/10.1007/s11244-022-01718-y.

Acknowledgements The authors acknowledge the financial support of the Initiative and Networking Fund of the Helmholtz Association through a Grant HRSF-0046. We acknowledge DESY (Hamburg, Germany), a member of the Helmholtz Association HGF, for the provision of experimental facilities. Parts of this research were carried out at PETRA III, and we would like to thank Dr. Wolfgang Caliebe (DESY) for assistance in using P64 beamline. Beamtime was allocated for proposal I-20200270. The authors acknowledge China Scholarship Council (CSC) who funded PhD studies of Xiaohui Huang at the Karlsruhe Nano Micro Facility (KNMF) where the TEM images were taken. We thank Dr. Di Wang (INT, KIT) for supervising the TEM experiments. The authors are grateful to Dr. Paolo Dolcet and Simon Barth (ITCP and IKFT respectively, KIT) for their help during synchrotron measurements, Dr. Andrey I. Stadnichenko, Dr. Lidiya S. Kibis, Dr. Dmitry A. Svintsitskiy, and Dr. Andrei I. Boronin (Boreskov Institute of Catalysis, Novosibirsk) for scientific discussions and project planning.

Funding Open Access funding enabled and organized by Projekt DEAL.

Declarations

Conflict of interest The authors have no competing interests to declare that are relevant to the content of this article.

References

1. Long RQ, Yang RT (2001) Selective catalytic oxidation (SCO) of ammonia to nitrogen over Fe-exchanged zeolites. J Catal 201(1):145–152. https://doi.org/10.1006/jcat.2001.3234
2. Chmielarz L, Jabłońska M (2015) Advances in selective catalytic oxidation of ammonia to dinitrogen: a review. RSC Adv 5(54):43408–43431. https://doi.org/10.1039/C5RA03218K
3. Long RQ, Yang RT (2002) Noble metal (Pt, Rh, Pd) promoted Fe-ZSM-5 for selective catalytic oxidation of ammonia to N_2 at low temperatures. Catal Lett 78(1):353–357. https://doi.org/10.1023/A:1014929222854
4. Jabłońska M (2021) Progress on noble metal-based catalysts dedicated to the selective catalytic ammonia oxidation into nitrogen and water vapor (NH3-SCO). Molecules 26(21):6461. https://doi.org/10.3390/molecules26216461
5. Lezcano-Gonzalez I, Deka U, van der Bij HE, Paalanen P, Arstad B, Weckhuysen BM, Beale AM (2014) Chemical deactivation of Cu-SSZ-13 ammonia selective catalytic reduction (NH3-SCR) systems. Appl Catal B 154:339–349. https://doi.org/10.1016/j.apcatb.2014.02.037
6. Chmielarz L, Jabłońska M, Strumiński A, Piwowarska Z, Węgrzyn A, Witkowski S, Michalik M (2013) Selective catalytic oxidation of ammonia to nitrogen over Mg-Al, Cu-Mg-Al and Fe-Mg-Al mixed metal oxides doped with noble metals. Appl Catal B 130–131:152–162. https://doi.org/10.1016/j.apcatb.2012.11.004
7. Zhao HW, Han L, Wang YJ, Zheng JD (2021) Insight into platinum poisoning effect on Cu-SSZ-13 in selective catalytic reduction of NO_x with NH3. Catalysts 11(7):796. https://doi.org/10.3390/catal11070796
8. Shrestha S, Harold MP, Kamasamudram K, Yezerets A (2013) Ammonia oxidation on structured composite catalysts. Top Catal 56(1–8):182–186. https://doi.org/10.1007/s11244-013-9949-9
9. Shrestha S, Harold MP, Kamasamudram K, Yezerets A (2014) Selective oxidation of ammonia on mixed and dual-layer Fe-ZSM-5 + Pt/Al_2O_3 monolithic catalysts. Catal Today 231:105–115. https://doi.org/10.1016/j.cattod.2014.01.024
10. Scheuer A, Hauptmann W, Drochner A, Gieshoff J, Vogel H, Votsmeier M (2012) Dual layer automotive ammonia oxidation catalysts: experiments and computer simulation. Appl Catal B 111–112:445–455. https://doi.org/10.1016/j.apcatb.2011.10.032
11. Ghosh RS, Le TT, Terlier T, Rimer JD, Harold MP, Wang D (2020) Enhanced selective oxidation of ammonia in a Pt/Al_2O_3@Cu/ZSM-5 core–shell catalyst. ACS Catal 10(6):3604–3617. https://doi.org/10.1021/acscatal.9b04288
12. Colombo M, Nova I, Tronconi E, Schmeißer V, Bandl-Konrad B, Zimmermann L (2013) Experimental and modeling study of a dual-layer (SCR + PGM) NH_3 slip monolith catalyst (ASC) for automotive SCR aftertreatment systems. Part 1. Kinetics for the PGM component and analysis of SCR/PGM interactions. Appl Catal B 142–143:861–876. https://doi.org/10.1016/j.apcatb.2012.10.031
13. Shrestha S, Harold MP, Kamasamudram K, Kumar A, Olsson L, Leistner K (2016) Selective oxidation of ammonia to nitrogen on bi-functional Cu-SSZ-13 and Pt/Al_2O_3 monolith catalyst. Catal Today 267:130–144. https://doi.org/10.1016/j.cattod.2015.11.035
14. Colombo M, Nova I, Tronconi E, Schmeißer V, Bandl-Konrad B, Zimmermann LR (2013) Experimental and modeling study of a dual-layer (SCR + PGM) NH_3 slip monolith catalyst (ASC) for automotive SCR after treatment systems. Part 2. Validation of PGM kinetics and modeling of the dual-layer ASC monolith. Appl Catal B 142–143:337–343. https://doi.org/10.1016/j.apcatb.2013.05.032
15. Dhillon PS, Harold MP, Wang D, Kumar A, Joshi SY (2019) Enhanced transport in washcoated monoliths: application to selective lean NO_x reduction and ammonia oxidation. Chem Eng J 377:119734. https://doi.org/10.1016/j.cej.2018.08.120
16. Kim MS, Lee DW, Chung SH, Hong YK, Lee SH, Oh SH, Cho IH, Lee KY (2012) Oxidation of ammonia to nitrogen over Pt/Fe/ZSM5 catalyst: influence of catalyst support on the low temperature activity. J Hazard Mater 237:153–160. https://doi.org/10.1016/j.jhazmat.2012.08.026
17. Oh SH, Cavendish JC (1982) Transients of monolithic catalytic converters. Response to step changes in feedstream temperature as related to controlling automobile emissions. Ind Eng Chem Product Res Dev 21(1):29–37. https://doi.org/10.1021/i300005a006
18. Robinson K, Ye S, Yap Y, Kolaczkowski ST (2013) Application of a methodology to assess the performance of a full-scale diesel oxidation catalyst during cold and hot start NEDC drive cycles. Chem Eng Res Des 91(7):1292–1306. https://doi.org/10.1016/j.cherd.2013.02.022
19. Weisweiler W, Wunsch R (1998) Simulation of a driving cycle in laboratory: an approach for testing catalysts suitable for automotive exhaust NO_x abatement under lean conditions. Chem Eng Process Process Intensif 37(3):229–232. https://doi.org/10.1016/S0255-2701(98)00027-0
20. Scheuer A, Votsmeier M, Schuler A, Gieshoff J, Drochner A, Vogel H (2009) NH3-Slip catalysts: experiments versus mechanistic modelling. Top Catal 52(13–20):1847–1851. https://doi.org/10.1007/s11244-009-9351-9
21. Maurer F, Jelic J, Wang J, Gänzler A, Dolcet P, Wöll C, Wang Y, Studt F, Casapu M, Grunwaldt J-D (2020) Tracking the formation, fate and consequence for catalytic activity of Pt single sites on CeO_2. Nat Catal 3(10):824–833. https://doi.org/10.1038/s41929-020-00508-7
22. Casapu M, Fischer A, Gänzler AM, Popescu R, Crone M, Gerthsen D, Turk M, Grunwaldt J-D (2017) Origin of the normal and inverse hysteresis behavior during CO oxidation over Pt/Al_2O_3. ACS Catal 7(1):343–355. https://doi.org/10.1021/acscatal.6b02709
23. Boubnov A, Carvalho HWP, Doronkin DE, Günter T, Gallo E, Atkins AJ, Jacob CR, Grunwaldt J-D (2014) Selective catalytic reduction of NO over Fe-ZSM-5: mechanistic insights by Operando HERFD-XANES and valence-to-core X-ray emission spectroscopy. J Am Chem Soc 136(37):13006–13015. https://doi.org/10.1021/ja5062505

24. Lu Y, Santhosh Kumar M, Chiarello GL, Dimopoulos Eggenschwiler P, Bach C, Weilenmann M, Spiteri A, Weidenkaff A, Ferri D (2013) Operando XANES study of simulated transient cycles on a Pd-only three-way catalyst. Catal Commun 39:55–59. https://doi.org/10.1016/j.catcom.2013.05.006
25. Balakotaiah V, Sun Z, Ratnakar R (2021) Ignition-extinction analysis of catalytic reactor models. Rev Chem Eng. https://doi.org/10.1515/revce-2020-0113
26. Tutuianu M, Bonnel P, Ciuffo B, Haniu T, Ichikawa N, Marotta A, Pavlovic J, Steven H (2015) Development of the World-wide harmonized Light duty Test Cycle (WLTC) and a possible pathway for its introduction in the European legislation. Transp Res D Transp Environ 40:61–75. https://doi.org/10.1016/j.trd.2015.07.011
27. Opitz B, Bendrich M, Drochner A, Vogel H, Hayes RE, Forbes JF, Votsmeier M (2015) Simulation study of SCR catalysts with individually adjusted ammonia dosing strategies. Chem Eng J 264:936–944. https://doi.org/10.1016/j.cej.2014.11.114
28. Pontikakis GN, Konstantas GS, Stamatelos AM (2004) Three-way catalytic converter modeling as a modern engineering design tool. J Eng Gas Turbines Power 126(4):906–923. https://doi.org/10.1115/1.1787506
29. Bendrich M, Opitz B, Scheuer A, Hayes RE, Votsmeier M (2021) Selective catalytic reduction: adding an ammonia slip catalyst mitigates dosing errors. Can J Chem Eng 100:1439–1447. https://doi.org/10.1002/cjce.24293
30. Benzi F, Sheppard TL, Doronkin DE, Meira DM, Gänzler AM, Baier S, Grunwaldt J-D (2017) Transient structural and catalytic behaviour of Pt-particles probed by operando spectroscopy during a realistic driving cycle. Catal Sci Technol 7(18):3999–4006. https://doi.org/10.1039/C7CY00926G
31. Doronkin DE, Baier S, Sheppard T, Benzi F, Grunwaldt J-D (2016) Lithographically fabricated silicon microreactor foroperando QEXAFS studies in exhaust gas catalysis during simulation of a standard driving cycle. J Phys: Conf Ser 712:012030. https://doi.org/10.1088/1742-6596/712/1/012030
32. Abramoff M, Magalhães P, Ram SJ (2003) Image processing with ImageJ. Biophotonics Int 11:36–42
33. Bornmann B, Kläs J, Müller O, Luetzenkirchen-Hecht D, Frahm R (2019) The quick EXAFS setup at beamline P64 at PETRA III for up to 200 spectra per second. AIP Conf Proc 2054: 040008. https://doi.org/10.1063/1.5084609
34. Ravel B, Newville M (2005) ATHENA, ARTEMIS, HEPHAESTUS: data analysis for X-ray absorption spectroscopy using IFEFFIT. J Synchrotron Radiat 12:537–541. https://doi.org/10.1107/S0909049505012719
35. Grunwaldt J-D, Caravati M, Hannemann S, Baiker A (2004) X-ray absorption spectroscopy under reaction conditions: suitability of different reaction cells for combined catalyst characterization and time-resolved studies. Phys Chem Chem Phys 6(11):3037–3047. https://doi.org/10.1039/B403071K
36. Kumar MS, Schwidder M, Grünert W, Brückner A (2004) On the nature of different iron sites and their catalytic role in Fe-ZSM-5 DeNO$_x$ catalysts: new insights by a combined EPR and UV/VIS spectroscopic approach. J Catal 227(2):384–397. https://doi.org/10.1016/j.jcat.2004.08.003
37. Pérez-Ramírez J, Gallardo-Llamas A (2005) Impact of the preparation method and iron impurities in Fe-ZSM-5 zeolites for propylene production via oxidative dehydrogenation of propane with N_2O. Appl Catal A: Gen 279(1):117–123. https://doi.org/10.1016/j.apcata.2004.10.020
38. Doronkin DE, Casapu M, Gunter T, Muller O, Frahm R, Grunwaldt JD (2014) Operando spatially- and time-resolved XAS study on zeolite catalysts for selective catalytic reduction of NO_x by NH_3. J Phys Chem C 118(19):10204–10212. https://doi.org/10.1021/jp5028433
39. Singh J, Alayon EMC, Tromp M, Safonova OV, Glatzel P, Nachtegaal M, Frahm R, van Bokhoven JA (2008) Generating highly active partially oxidized platinum during oxidation of carbon monoxide over Pt/Al_2O_3: in situ, time-resolved, and high-energy-resolution X-ray absorption spectroscopy. Angew Chem Int Ed 47(48):9260–9264. https://doi.org/10.1002/anie.200803427
40. Petit PE, Farges F, Wilke M, Sole VA (2001) Determination of the iron oxidation state in Earth materials using XANES pre-edge information. J Synchrotron Radiat 8:952–954. https://doi.org/10.1107/S0909049500021063
41. Boubnov A, Lichtenberg H, Mangold S, Grunwaldt JD (2015) Identification of the iron oxidation state and coordination geometry in iron oxide- and zeolite-based catalysts using pre-edge XAS analysis. J Synchrotron Radiat 22:410–426. https://doi.org/10.1107/S1600577514025880
42. Castoldi L, Bonzi R, Lietti L, Forzatti P, Morandi S, Ghiotti G, Dzwigaj S (2011) Catalytic behaviour of hybrid LNT/SCR systems: reactivity and in situ FTIR study. J Catal 282(1):128–144. https://doi.org/10.1016/j.jcat.2011.06.002
43. Krivoruchenko DS, Kucherov AV, Telegina NS, Bokarev DA, Selvam P, Stakheev AY (2014) Development of the bifunctional catalyst Mn-Fe-Beta for selective catalytic reduction of nitrogen oxides. Russ Chem Bull 63(2):389–395. https://doi.org/10.1007/s11172-014-0442-9
44. Kalz KF, Kraehnert R, Dvoyashkin M, Dittmeyer R, Glaser R, Krewer U, Reuter K, Grunwaldt J-D (2017) Future challenges in heterogeneous catalysis: understanding catalysts under dynamic reaction conditions. ChemCatChem 9(1):17–29. https://doi.org/10.1002/cctc.201600996